Deep Mining 2024 – P Andrieux & D Cumming-Potvin (eds)

doi:10.36487/ACG_repo/2465_15

Hazard identification and mitigation using numerical modelling and seismic data analyses in an underground gold mine

Colin Hume [a,*], Kathy Kalenchuk [a], Neda Dadashzadeh [a]

[a] *RockEng Inc., Canada*

Abstract

The management of risk associated with mine-induced stress and associated ground response in underground mines is a necessary component for ensuring the safety of underground mining personnel as well as the economic viability of underground ore recovery. Numerical models can be very powerful methods for investigating and evaluating geomechanical hazards associated with induced stress in underground mines. When effectively calibrated, numerical models can provide the means for reliable engineered predictions of ground reaction in response to future mining. Seismic monitoring provides essential data to characterise the seismogenic rock mass response and also provides the basis for quantitative model calibration as well as domain-based analyses of seismic hazard spatially throughout a mine and temporally during mining activities. This paper presents a case study of a mine where adverse seismicity and rockbursting halted production in a critical mining zone in 2023. Numerical modelling and seismic data interpretations were then relied upon for event back-analyses and the development of tactical and strategic risk mitigation measures for managing potential future seismic hazards. A discussion of numerical model calibration is presented, with numerical outputs generated by the simulation of historical mining activity systematically reconciled against the available seismic history record. The process involved statistical evaluation of numerical outputs for seismogenic geotechnical domains as well as induced stress tensors evaluated against seismic source mechanisms. The calibrated numerical model is then used to understand geomechanical hazards associated with future mining plans.

Keywords: *numerical modelling, model calibration, seismic data analysis, mine-induced stress, underground mining, case study*

1 Introduction

This paper provides a case study where a significant unusual ground occurrence (UGO) in a sill pillar mining horizon resulted in the suspension of mining activities on several mining levels near to the occurrence location. This prompted an investigation to determine contributing factors and to evaluate the potential for similar geomechanical hazards during continued mining in the same, and other, sill pillars in the underground operation. The investigation involved two components: seismic data analysis and numerical modelling analysis. Seismic data interpretation and analysis have been used to understand the expected rock mass response to loading conditions based on the observed ground reaction. Numerical modelling analysis involved using calibrated models to interpret the contribution of stress conditions to the UGO.

1.1 Geological setting

The mining operation is located in an Archean-aged greenstone belt. The narrow vein gold deposit is hosted within metavolcanic (mafic and ultramafic) and clastic metasedimentary rock units. The occurrence of

* Corresponding author.

graphitic and pyritic mudstone is also a distinctive rock type that is generally found along or within several hundred metres of the contact with mafic metavolcanic rock (graphite zone). The rock mass of the deposit is consistently foliated, with foliation-related joint spacing steeply dipping to the south and observed to have small (mm-scale) spacing up to the metre scale. Mineralisation is generally parallel to foliation.

1.2 Mining setting

The underground mine primarily utilises longitudinal longhole open stoping; transverse stoping is locally implemented where better suited based on wider orebody geometry. Sills are developed in ore (on geology control) from a central access to the lateral (west and east) extents of the deposit and the stopes are retreated from the extents towards the access. Production at the time of the UGO ranged between 400 m and 1,345 m below ground surface (mbgs). Level spacing above 1,000 mbgs ranges from 15 to 18 m, and below 1,000 mbgs range from 20 to 23 m. Strike lengths for stopes are typically 20 m. The resource is mined top down in blocks comprising three or four sublevels, with each individual block being mined bottom up, resulting in diminishing sill pillars.

1.3 Geomechanical site characterisation

Intact rock testing and field observations of intact rock strength have demonstrated moderate variability in intact material strength; the unconfined compressive strengths (UCS) of the major lithologies range from 100 to 130 MPa. Limited rock testing was available for the site and some of the data does not distinguish rock types; consequently, the testing data are grouped together for all of the rock types. Rock mass quality has been evaluated by various underground mapping campaigns. The Q' ratings (the modified Q-value, as presented by Hoek et al. 1995) range from Q' = 7.1 to 22. Four main joint sets are observed throughout the mine as follows:

- a dominant set steeply dipping to the south and associated with foliation
- a sub-horizontal set
- a sub-vertical, weakly defined set striking southeast to northwest
- a weakly defined set steeply dipping to the east.

1.4 In situ stress

No stress testing has been completed at the mine so regional data is relied on to establish an assumed base case in situ stress tensor as provided in Table 1.

Table 1 Regional stress tensor and range of magnitudes assumed for the numerical analyses

	Principal stress component		
	σ_1	σ_2	σ_3
Orientation (dip/dip direction)	0°/090°	0°/000°	90°/000°
Magnitude (MPa)	2.0 σ_3	1.6 σ_3	0.027 z
z is the depth in metres below surface			

1.5 Summary of recent unusual ground occurrence

The UGO involved a floorburst event within a crosscut of a transverse stoping area within a sill pillar at 1,185 mbgs. The floorburst damage was observed over a 10 m length of drift, with floor lift in the order of 0.5 m (Figure 1). This damage was attributed to a large seismic event located in the area. Field inspection identified significant stress damage and ground support loading throughout this sill pillar level. It was

observed that damage was prevalent along a low-angle structure observed in the 1,185 mbgs sill tracing through the floorburst location (Figure 2).

Figure 1 Photo showing floorburst damage

Figure 2 Photo of low-angle structures on walls of 1,185 mbgs sill at the floorburst location

Preliminary seismic data review established a conceptual mechanism model whereby the triggering seismic event (as well as other macro-events observed in the area) were likely associated with a stress-induced slip of a shallow southeast-dipping structural trend. The geological nature of this structural trend was unknown at the time of investigation so it has been referred to as a 'structural corridor'. In order to establish risk-mitigating control with ongoing extraction in the area it was necessary to further understand the underlying mechanisms contributing to the occurrence and identify the potential for manifestation of similar hazards in the future.

2 Seismic data analysis

To quantify seismic hazard and forecast future risk, seismic data analyses were required to investigate the mechanisms of rock mass response to mining-induced loading conditions. As a general best practice in operational ground control, comprehensive reviews of historical ground responses, UGOs and seismicity offer insight into the rock mass failure processes and how rock failure can manifest as excavation damage. This provides necessary inputs to achieve engineering designs and informed decision-making pertaining to strategic and tactical risk mitigation.

Seismic data analyses were completed using mXrap software. The mXrap project was constructed from:

- seismic data of the seismic monitoring system
- available lithological wireframes
- as-built mine geometries
- planned life of mine stope shapes
- production blast indicators over a two-year monitoring period.

Magnitude values in this paper are expressed as local magnitude (ML) and, in the context of this report, large events refer to seismic events with ML > 0.0.

2.1 Seismic system overview

The seismic monitoring system at this operation detects and measures seismicity through an array of four triaxial geophones and four uniaxial geophones (Figure 3). Sensors are installed between 1,095 and 1,250 mbgs.

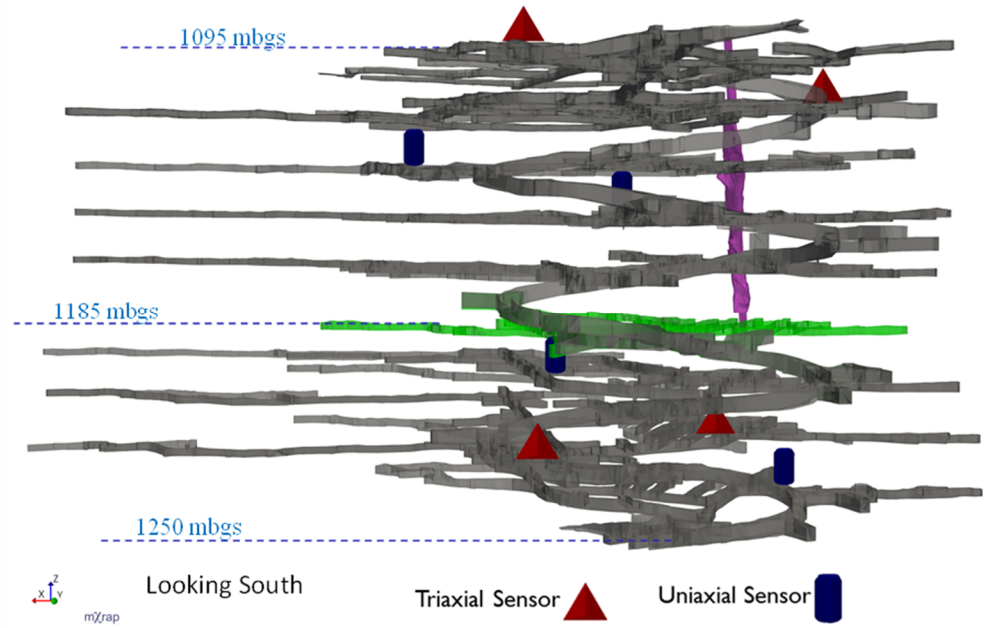

Figure 3 Seismic array of case study

2.2 Quality review of seismic data and system array

Data quality assessments were completed to identify any possible errors with associated data and/or system hardware/software. System sensitivity, event location accuracy, sources of noise and the quality of source parameter measurements were investigated.

2.2.1 System sensitivity

The sensitivity of the seismic system is defined as the minimum magnitude event (of derived ML) that is reliably measured and recorded by the system (Mmin). Iso-surfaces of Mmin relevant to the underground mine are shown in Figure 4. The greatest sensitivity of the system is between 1,120 mbgs and 1,250 mbgs in the footwall development. In the UGO area of interest the system can observe events to ML–2.0.

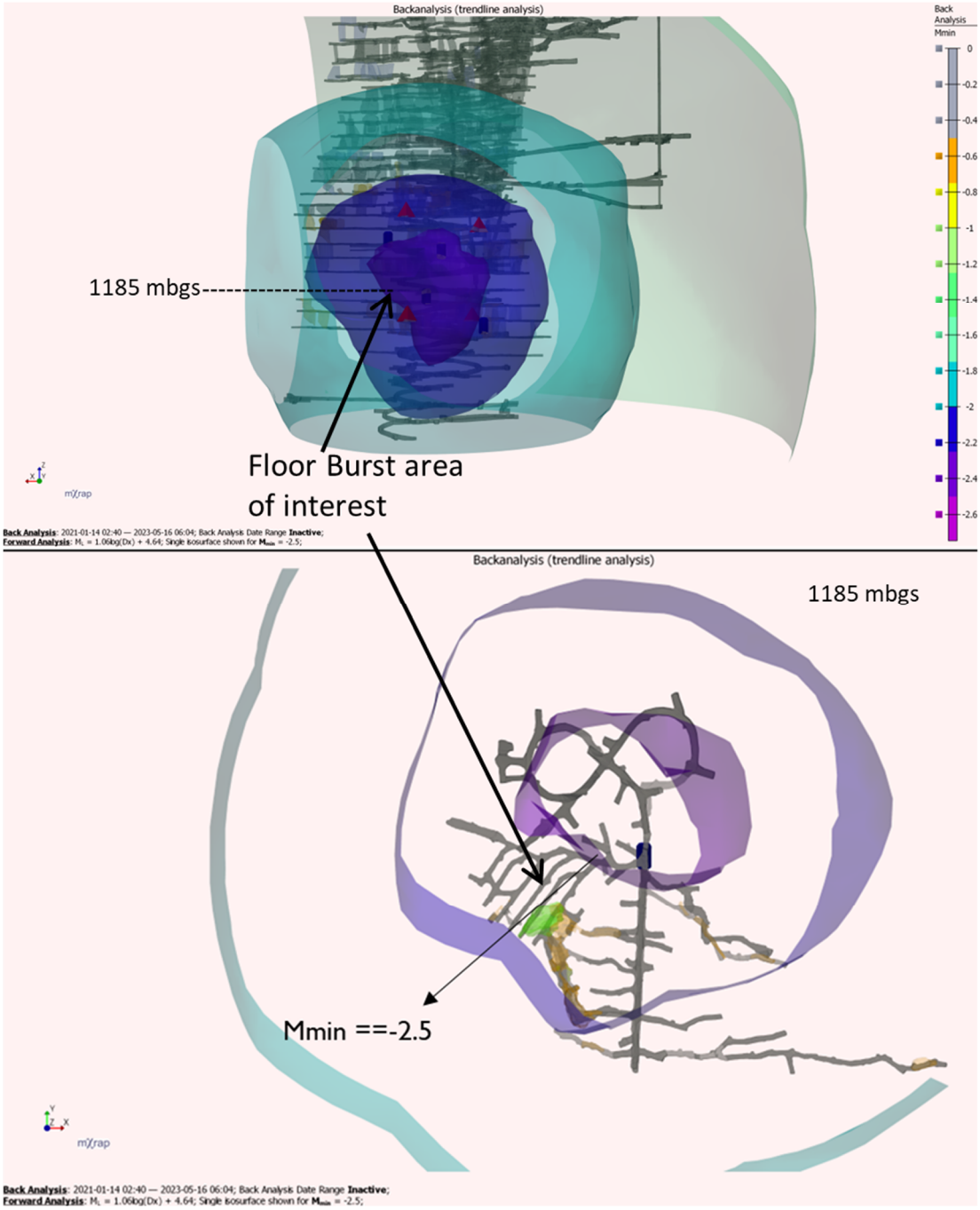

Figure 4 Seismic array sensitivity (Mmin being the smallest magnitude for ML that the seismic system can detect)

2.2.2 Event location accuracy

Location error describes the potential difference between the calculated location for a seismic event and the actual location of an event. Assessment of location error is typically interpreted through location residual parameter. Location residual is the mathematical error between the actual picks and where the location algorithm 'thinks' the pick should be. While location residual is not a direct measurement of location error, typically there is a correlation between location residual and accuracy. In this study the seismic dataset has been filtered to exclude events with a location residual > 20 m.

2.2.3 Sources of noise

Seismic data review identified data contamination near the ore handling infrastructure (crusher, rock passes/bins) associated with mechanical noise. Data in these areas were spatially filtered and removed from the dataset applied to seismic ground response analyses.

2.2.4 Seismic source parameter quality

Typically, source parameters for a given mine site should vary within consistent range limits. Distinct changes in measurement values can indicate potential systematic errors which may be associated with changes in hardware, software or data processing engines. For this case study an apparent drop in corner frequency measurements occurs after a certain date. Further, an apparent upper truncation of the frequency in the order of 2,500 Hz was observed in the database within the same time frame as the drop in corner frequency (Figure 5). These data irregularities were investigated and were found to be related to software settings which did not influence the study results.

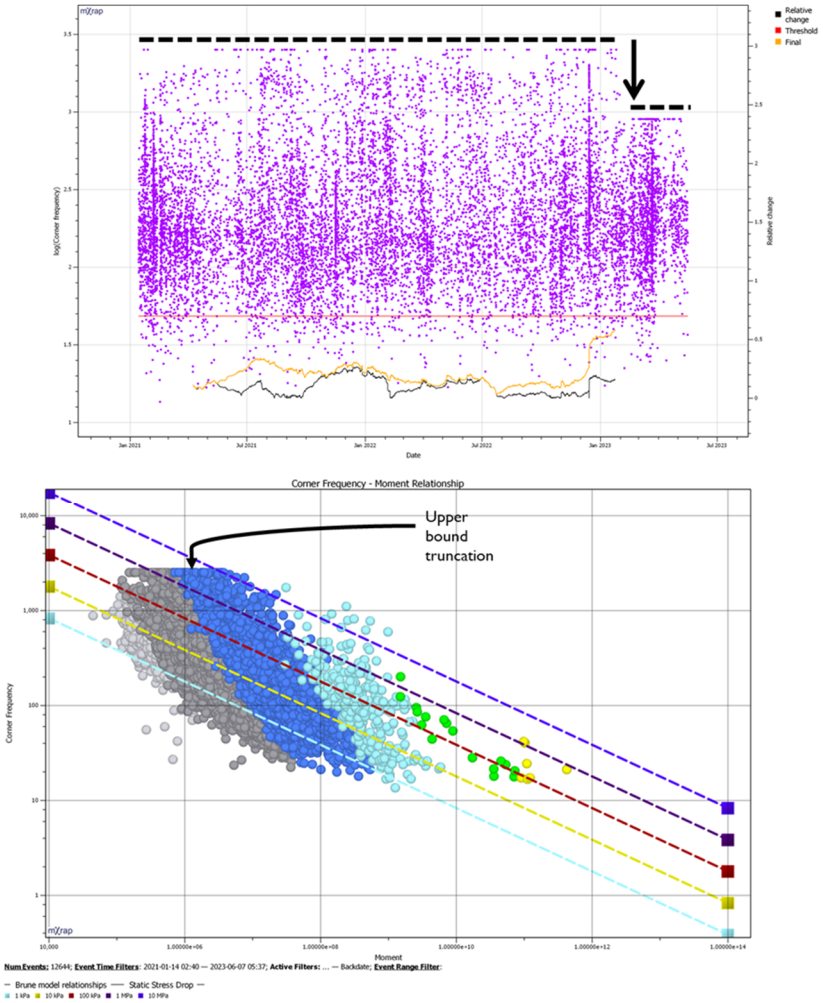

Figure 5 Observation of corner frequency drop in February 2023 and cut-off at 2,500 Hz

2.3 Seismic data analyses

2.3.1 Magnitude–time history

A magnitude–time history chart of all seismic events, including the cumulative number of events, daily activity histograms and a 30-day moving average analysis, is shown in Figure 6. Two short-term event rate increases are evident in the dataset leading up to the UGO floorburst event:

- On 14 December 2022 increased seismicity was observed within the sill pillar at 1,185 mbgs following a 7,000 tonne stope blast at 1,230 mbgs the day before this seismic activity increase. Shortly after the seismic activity increase an ML1.2 event occurred.
- On 21 March 2023 increased seismicity occurred again within the sill pillar at 1,185 mbgs following a 6,500 tonne stope blast at 1,205 mbgs the same day. Shortly after this seismic activity increase an ML0.4 event occurred. The floorburst damage was identified in the ore development at 1,185 mbgs during inspection after the ML0.4 event.

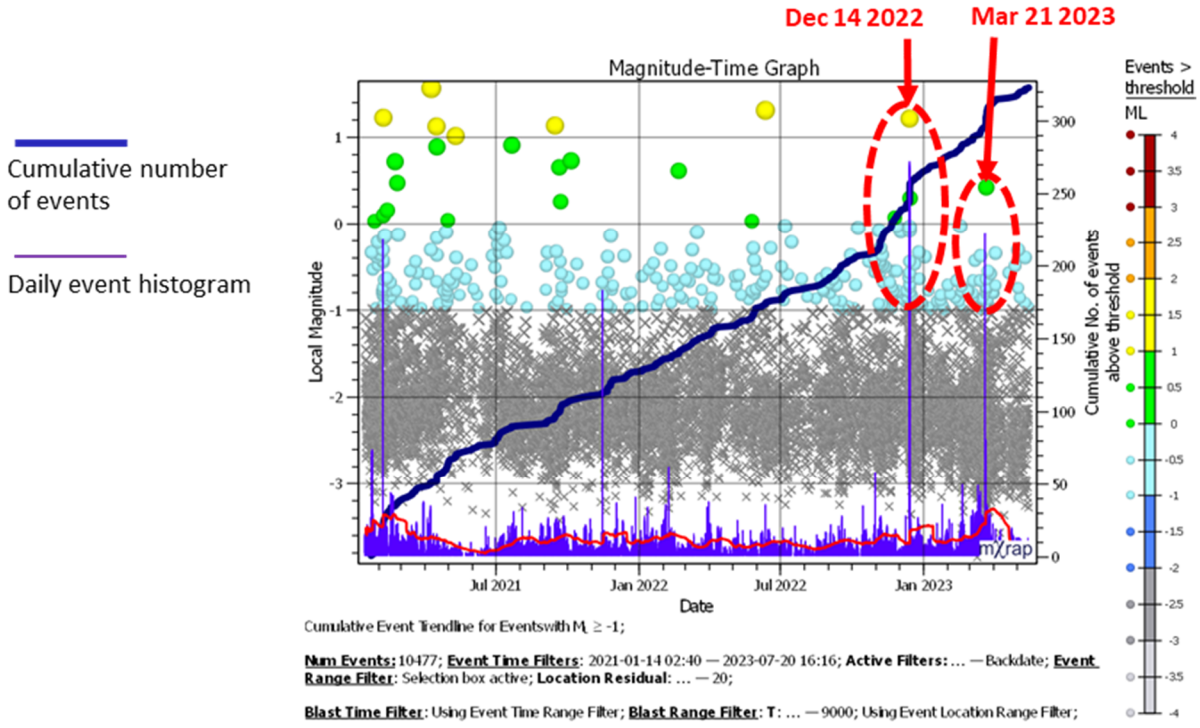

Figure 6 Magnitude–time analyses of seismic populations, with the cumulative number of events and daily event rate plots shown

2.4 Review of large seismic events

A total of 24 large seismic events (ML > 0.0) have been observed at the site and these are shown spatially in Figure 7. Five of these were located within the area of interest at 1,185 mbgs. A review of the seismic data and blasting records found that none of these events correlated well temporally and/or spatially with production activities.

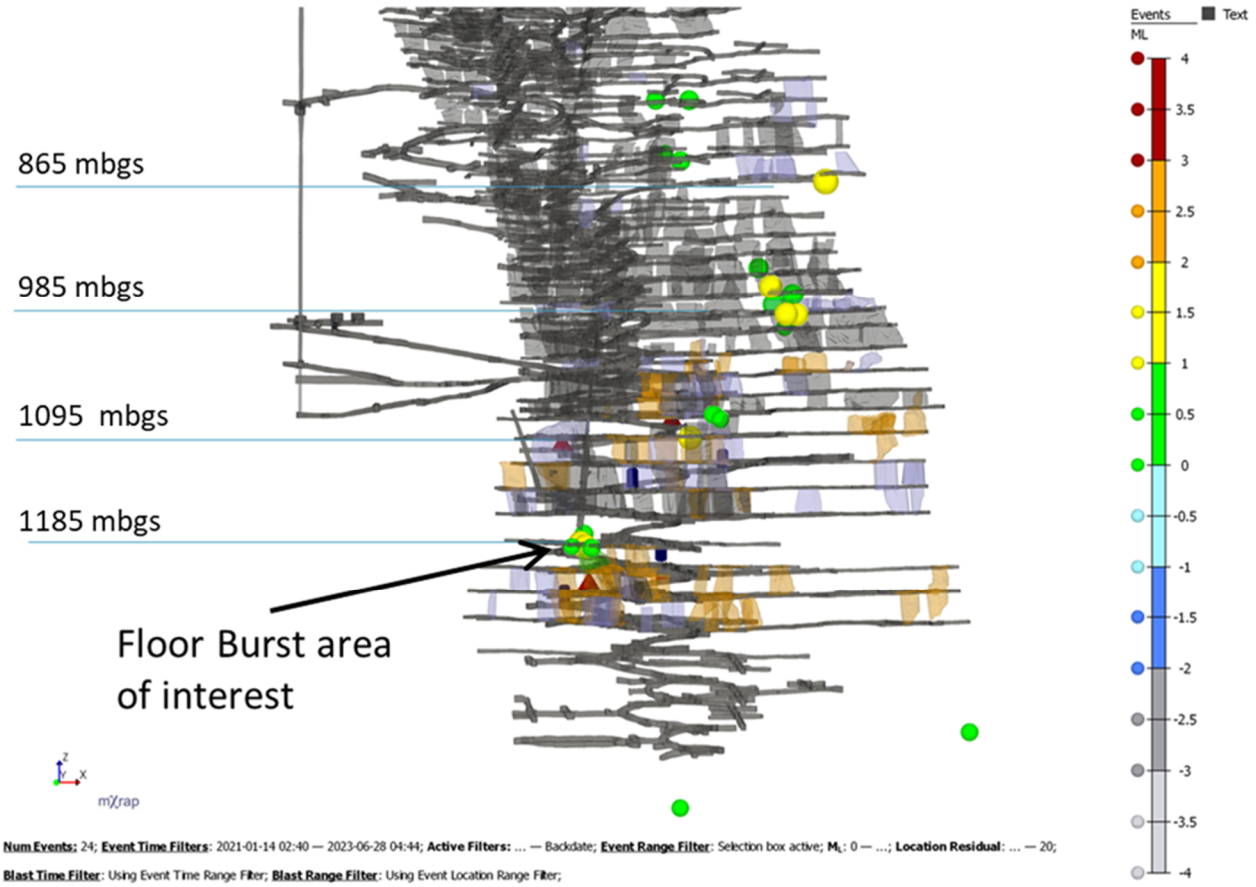

Figure 7 Overview of large magnitude seismicity (ML > 0.0)

2.5 General observations from mechanism analyses

A total of 98 moment tensor analyses were available for seismic events for the case study. The Hudson plot is shown in Figure 8, and stereonet analyses of double-couple (DC) nodal planes and principal axes are shown in Figure 9. Of interest to this study is the occurrence of a cluster of events occurring within the DC area which indicates potential structural dislocations. When graphed to a CLVD-ISO plot these events include shear cracking, which strengthens confidence in an interpretation of a structural failure mechanism that can induce seismic events as large as ML0.8. The ML0.4 event that was attributed to the floorburst has a complete shear mechanism (100% DC) confirming the occurrence of a structural slipping failure.

Upon review of the nodal plane stereonet it was found that the majority of the events with a slipping mechanism resolved as a shallow southeast-dipping displacement orientation (best-fit plane-3 in Figure 9).

It was further noted that the spatial distribution of seismicity at 1,185 mbgs generally produces a planar trend following a shallow southeast orientation, similar to the average nodal plane orientation and also to the shallow dipping structure observed in the 1,185 mbgs sill (Figure 2). This evidence supports the conceptual model of an apparent seismogenic structural corridor.

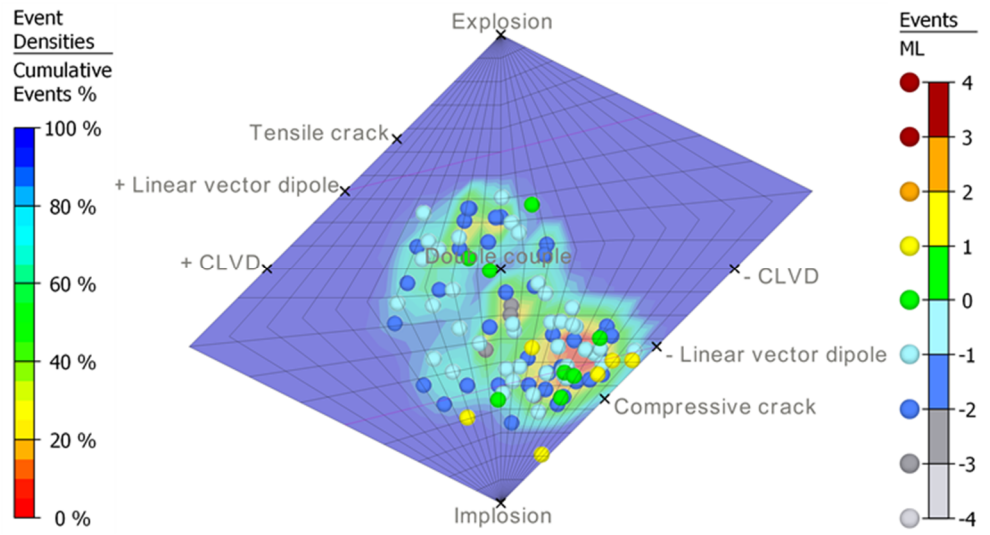

Figure 8 Mechanism analyses on the Hudson plot

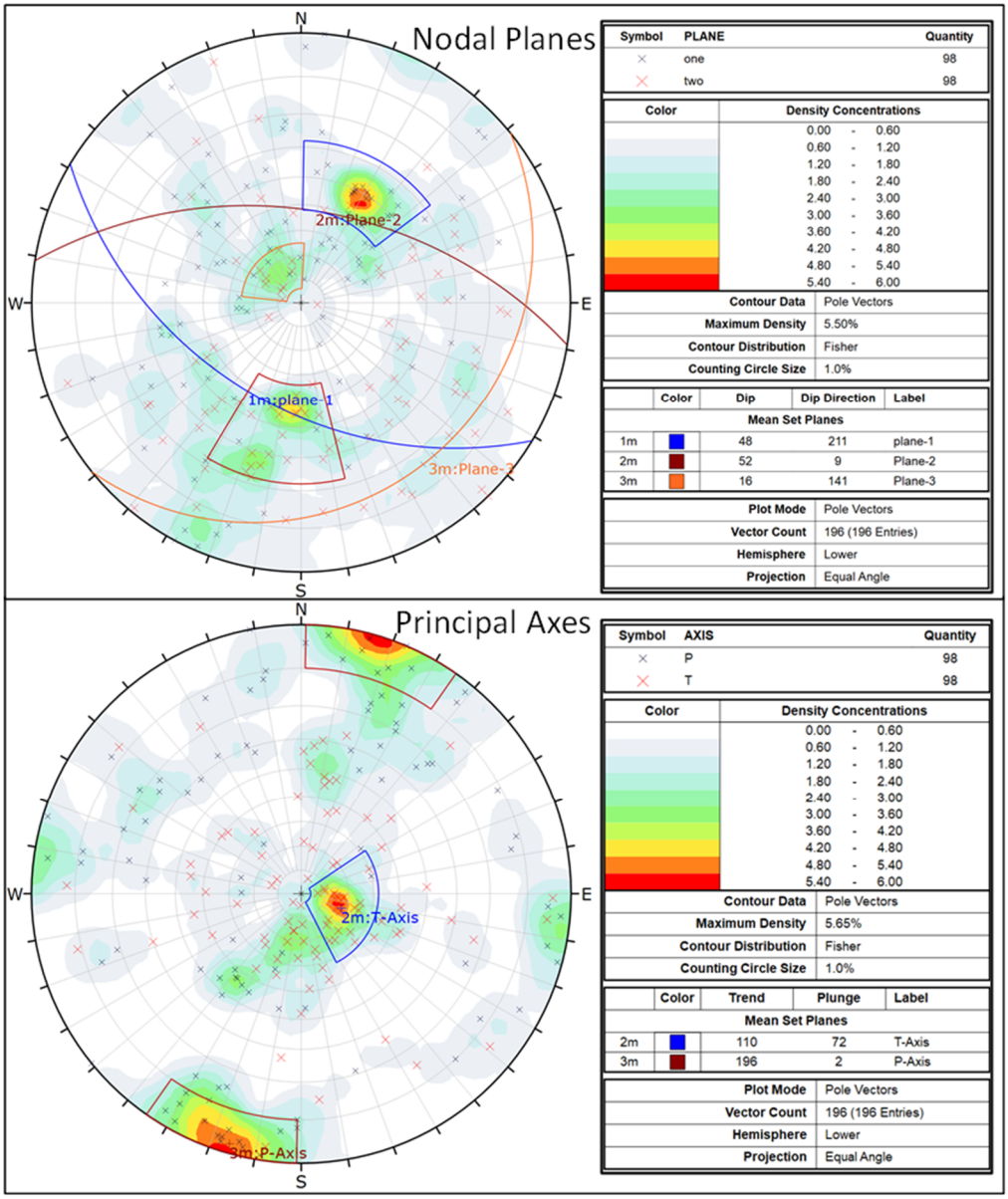

Figure 9 Best-fit stereonet analyses of DC nodal planes and principal axes

3 Numerical modelling analysis

Numerical modelling has been completed using the continuum-based, finite difference numerical code Fast Lagrangian Analysis of Continua in 3 Dimensions (FLAC3D) version 6.0 by Itasca Consulting Group (2016).

3.1 Numerical model input parameters

Major lithological domains represented in the numerical model were all defined assuming a perfectly plastic Hoek–Brown constitutive model, with the input parameters summarised in Table 2. As was noted in Section 1.3, some of the testing data does not distinguish rock types. Therefore an mi value of 10 was assumed for all rock types (in order to determine the mb parameter) and a Poisson's ratio value (v) of 0.25 was assumed. Backfill was represented as an elastic material.

Table 2 Summary of numerical model input parameters for each of the lithological domains represented in the numerical model

	Elastic properties			Strength properties			
Domain	E_{rm} (GPa)	*v*	ρ (g/cm^3)	σ_{ci} (MPa)	mb	s	a
Mafic volcanics (hanging wall, footwall)	16	0.25	2.83	100	3.0	0.0275	0.5
Sediments	9	0.25	2.83	100	2.0	0.007	0.5
Ultramafic (hanging wall)	16	0.25	2.83	100	2.4	0.0145	0.5
Graphite zone (hanging wall)	7	0.25	2.83	60	1.8	0.007	0.5
Backfill	1	0.25	1.80	N/A			

3.2 Numerical geometric representation and boundary conditions

A global numerical model representation of the mine has been approximated from the available cavity monitoring system survey and the development as-built shapes. A long section view of the stopes included in the numerical model in the lower portion of the mine is provided in Figure 10 (stopes included in the model extend to 400 mbgs). Major lithological units, which include the graphite zone, were defined.

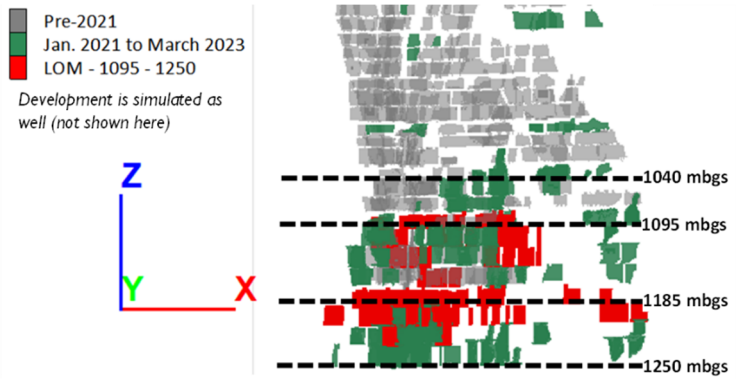

Figure 10 A long section of the numerical model representation of the stoping included in the numerical model (included development not shown)

The numerical model meshing scheme used in this study was an octree mesh, with localised and variable mesh refinement near the geometric boundaries dependent on the relevant area of interest and size of the geometry. A horizontal section of the numerical model at 1,095 mbgs showing the model geometry is presented in Figure 11, and includes the relative mesh sizing proximal to geometric boundaries.

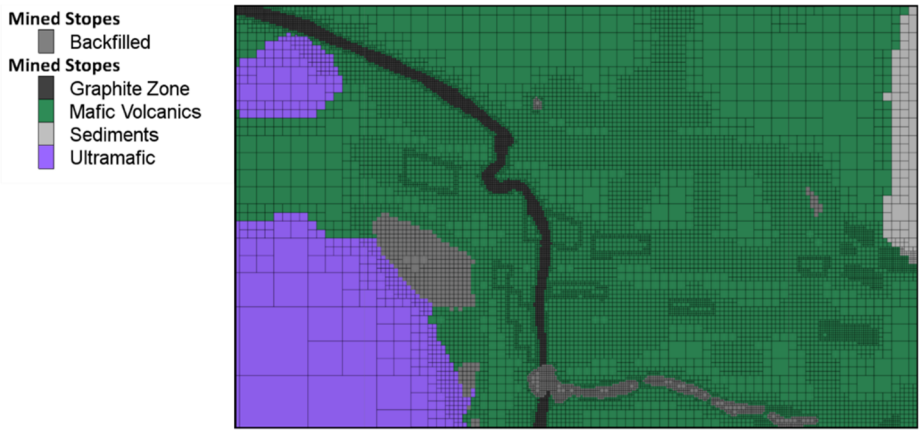

Figure 11 Horizontal section through 1,095 mbgs showing the geometry of stoping in major lithological units and stoping represented in the numerical model, including numerical mesh size (zones) relative to geometries of interest

The numerical model in this study has assumed a regional stress tensor as defined in Table 1. Stress was initialised to the numerical model using strain-based stress initialisation (Kalenchuk & Dadashzadeh 2022). A strain-based stress initialisation approach captures virgin state stress gradients associated with stiffness contrasts across the major lithological domains in the numerical model, with the goal that the strain applied to the model induces stress conditions that are more consistent with actual conditions that have developed over the geological history of the site. Figure 12 provides a horizontal cross-section through the numerical model at 1,040 mbgs to demonstrate the strain-based initialised pre-mining and non-uniform stress state.

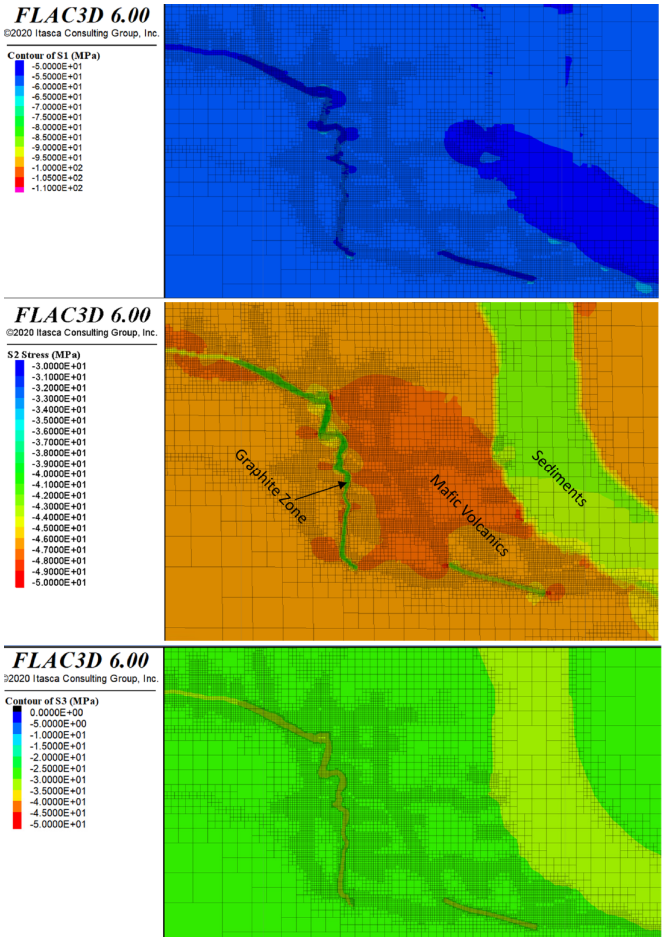

Figure 12 Horizontal section through 1,040 mbgs showing the numerically simulated virgin stress state for the strain-based stress initialisation

3.3 Statistical numerical model calibration

Calibration of the numerical model was completed using available seismic data for the mine (with the events filtered to remove mechanical noise, location residual > 20 m and ML < -2.0). Model calibration for this case study has utilised differential stress (σ_1–σ_3) to quantify a goodness of fit based on: (1) statistical repeatability of the stress state at seismic event locations, and (2) stress state magnitude relative to the UCS of each domain represented in the model following procedures described by Kalenchuk (2022). It is well established that the onset of microseismicity in the pre-peak regions of a rock mass begins when the stress state meets the damage threshold. A conceptual illustration is presented in Figure 13. Meeting this stress limit correlates to the onset of progressive damage and induced seismicity. The damage threshold can be simplified as a linear function (Martin 1994) as follows:

$$\sigma_{1crit} = A \cdot UCS + B \cdot \sigma_3 \quad (1)$$

where A generally varies between 0.3 and 0.5 depending on the rock type and B can be approximated as 1.0 (in the absence of robust laboratory testing). Ideally the statistical distribution of numerically predicted differential stress at seismic event locations in the pre-peak regions of a numerical model should have minimal variability within an individual domain and the largest portion of the data distribution should fall between the 0.3 UCS to 0.5 UCS for that given domain.

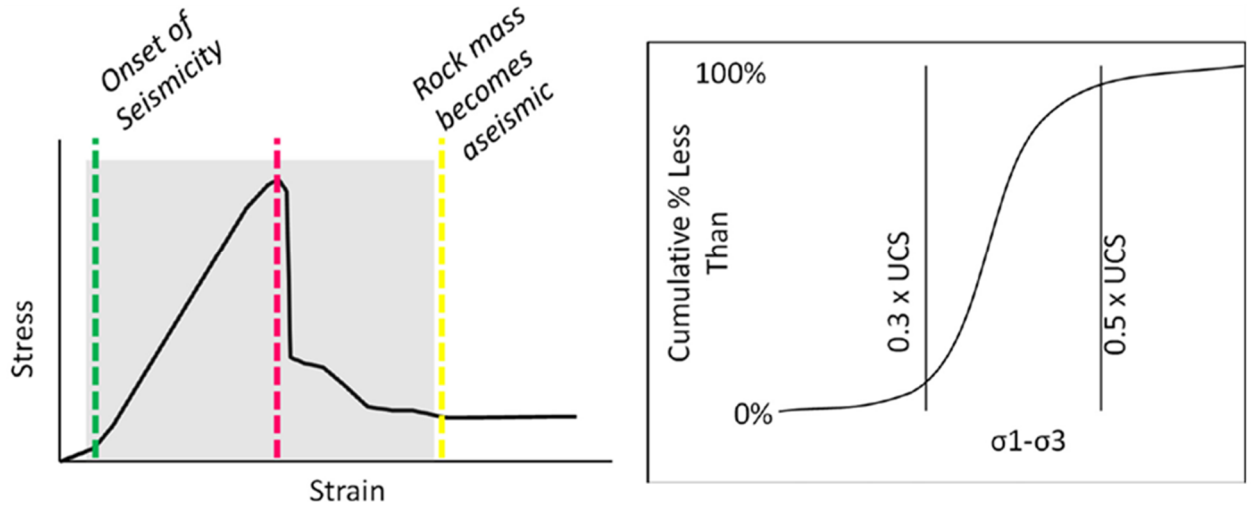

Figure 13 Correlation between differential stress and UCS for the seismic onset threshold

The statistical distributions of sampled differential stress (σ_1–σ_3) in the best calibrated model run (at the location of seismic events occurring in elastic regions of the numerical model) for the main lithological domain relevant to the mine (mafic volcanic host rock) are shown in Figure 14. Outlier data is noted in November and December 2022, and the spatial distribution of this outlier data is also shown in this figure. Interestingly, the outlier data is spatially correlated to a sill area at 1,185 mbgs where a structurally controlled seismic corridor has been identified (as noted in Section 2.5). The population produces a planar trend similar to the observed low-angle structures and nodal planes. This trend also agrees well with the interpretation of elevated apparent stress events in the area (though for brevity, apparent stress analyses of seismic events are not presented in this paper).

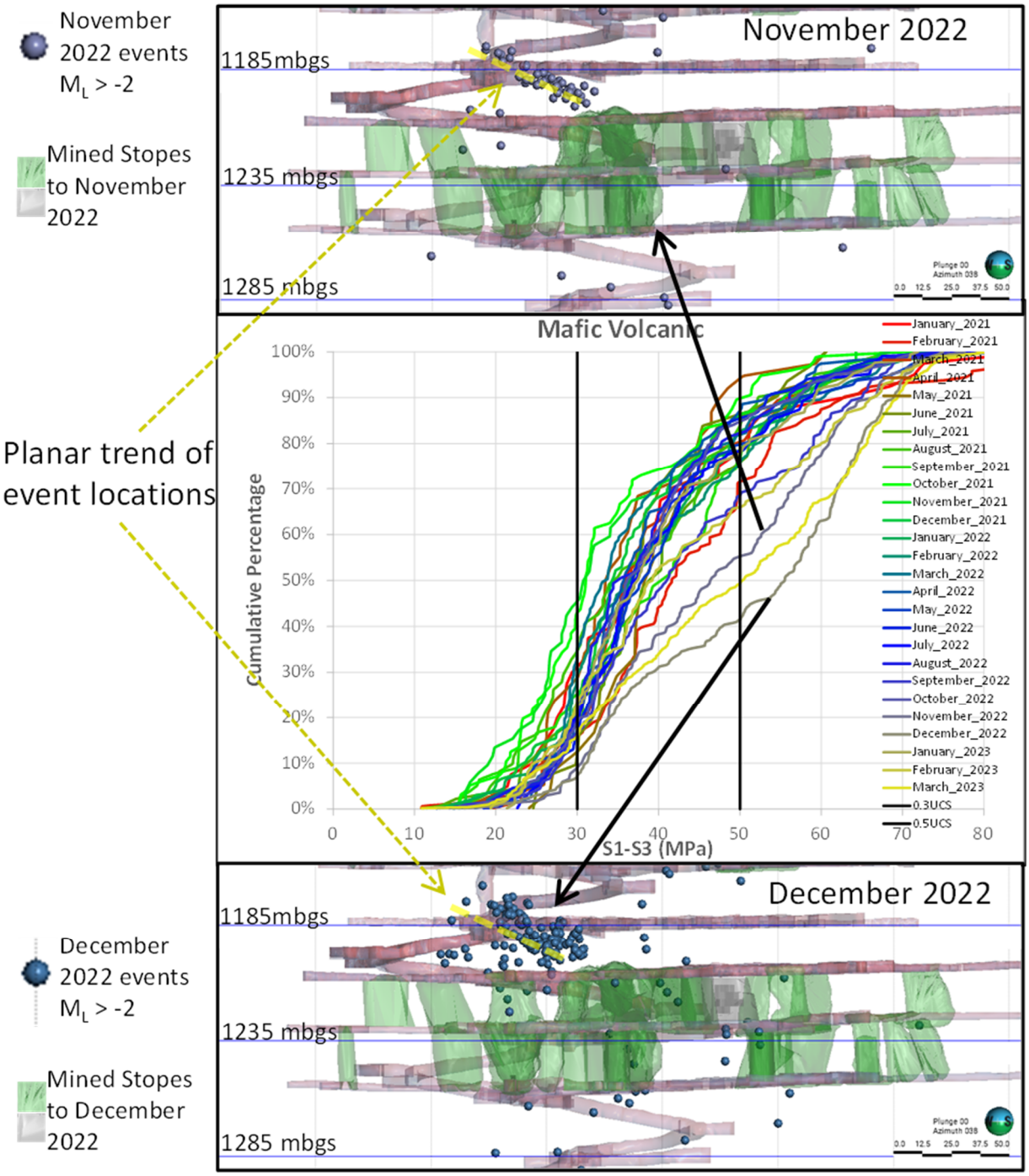

Figure 14 Statistical distribution of numerically predicted (σ_1–σ_3) at seismic event locations (data filtered for elastic regions of the model only) within the mafic volcanic domain

3.4 Qualitative verification of modelled stress

Stress damage observations at 1,185 mbgs were made during underground inspections. A qualitative comparison of the numerical model results to stress damage observations concluded that the stress magnitudes sampled within the pillar overlying level development provide reasonable correlation to no, low, moderate and heavy stress-induced damage. This qualitative comparison for the best calibrated model is shown in Figure 15, where regions of minor stress damage are indicated by 40 MPa ≤ (σ_1–σ_3) < 50 MPa, moderate are indicated by 50 MPa ≤ (σ_1–σ_3) < 60 MPa and heavy are indicated by (σ_1–σ_3) > 60 MPa or numerically predicted rock mass yield resulting from high stress.

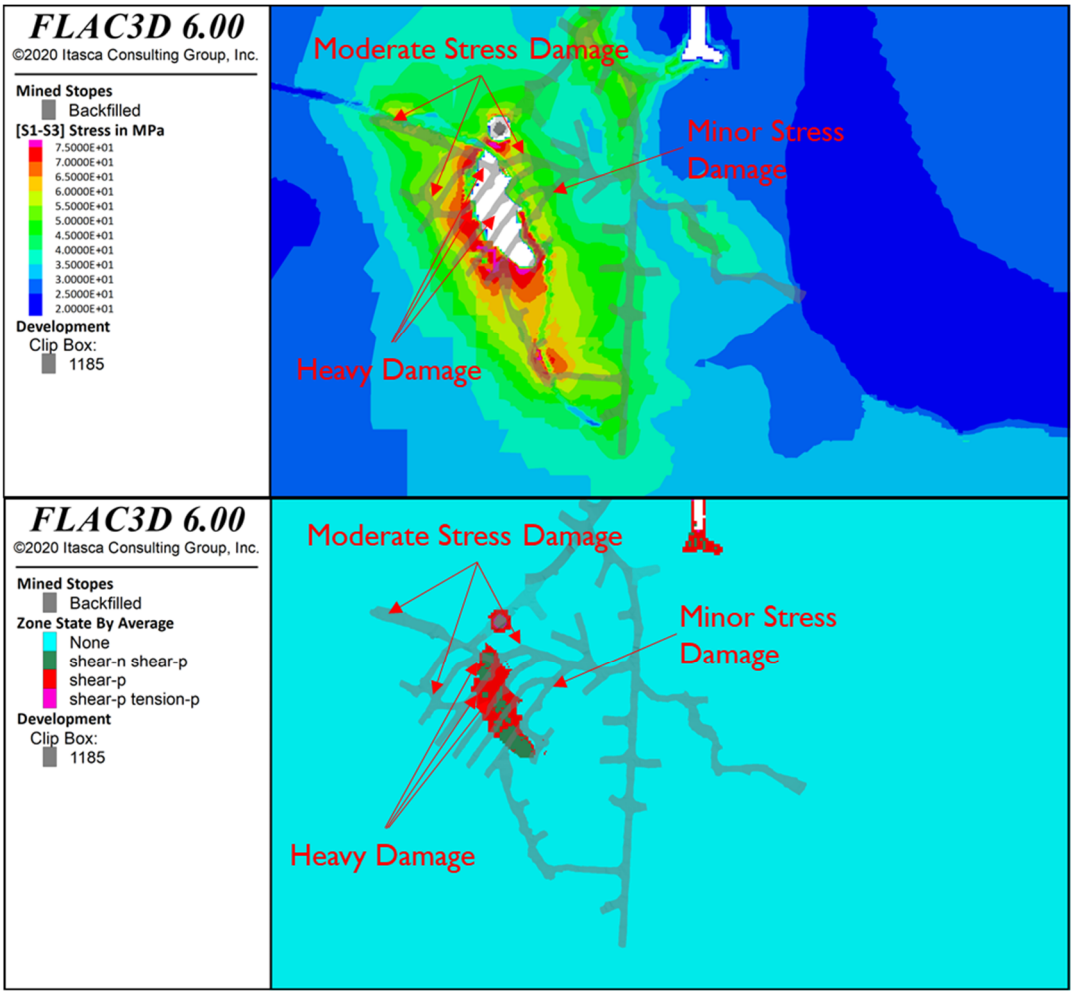

Figure 15 Horizontal section at mid-stope height above 1,185 mbgs showing (top) differential stress and (bottom) numerically predicted rock mass yield, with locations of qualitative damage observations noted

3.5 Numerical model back-analysis of the floorburst unusual ground occurrence

It was hypothesised that the floorburst identified at the 1,185 mbgs sill was a manifestation of a structural slip seismicity. As was discussed in Section 2.5, there were a number of events following a shallow southeast trend along seismic source locations (similar to the average nodal plane orientation).

The seismic corridor is not spatially associated with any modelled geological feature so has not been explicitly represented as a domain or structure in the numerical stress model. In the absence of explicit representation, the continuum model has been assessed to investigate whether the stress tensor conditions in the vicinity of this seismic trend suggest elevated susceptibility to potential slip behaviour. To do this, the full stress tensors for each zone in the model were resolved to the normal (σ_n) and shear (τ) stress components on planes with orientations corresponding to the average nodal planes of large events in the area.

The normal vector n to a plane (in Cartesian space) defined by dip (α) and dip direction (β) is determined from Equation 2.

$$\mathrm{n} = \begin{bmatrix} \sin \propto \sin \beta \\ \sin \propto \cos \beta \\ \cos \alpha \end{bmatrix} = \begin{bmatrix} n_1 \\ n_2 \\ n_3 \end{bmatrix} \quad (2)$$

The traction vector normal to this plane, $t^{(n)}$, is determined from the stress tensor σ and n from Equation 3.

$$\mathrm{t}^{(\mathrm{n})} = \begin{bmatrix} {t_1}^{(n)} \\ {t_2}^{(n)} \\ {t_3}^{(n)} \end{bmatrix} = \sigma\mathrm{n} = \begin{bmatrix} \sigma_1 & \sigma_{12} & \sigma_{13} \\ \sigma_{21} & \sigma_2 & \sigma_{23} \\ \sigma_{31} & \sigma_{32} & \sigma_3 \end{bmatrix} \begin{bmatrix} n_1 \\ n_2 \\ n_3 \end{bmatrix} \quad (3)$$

The magnitude of the normal stress acting on this plane (σ_n) is determined from Equation 4.

$$\sigma_n = \mathrm{t}^{(\mathrm{n})} \cdot \mathrm{n} = \begin{bmatrix} {t_1}^{(n)} \\ {t_2}^{(n)} \\ {t_3}^{(n)} \end{bmatrix} \begin{bmatrix} n_1 \\ n_2 \\ n_3 \end{bmatrix} = {t_1}^{(n)} \times n_1 + {t_2}^{(n)} \times n_2 + {t_3}^{(n)} \times n_3 \quad (4)$$

The magnitude of the shear stress acting on this plane (τ) is determined from Equation 5.

$$\tau = \sqrt{|\mathrm{t}^{(\mathrm{n})}|^2 - {\sigma_n}^2} \quad (5)$$

A Factor of Safety (FOS) calculation made by comparing this resolved σ_n and τ to a fixed strength criterion provides a relative indication of elevated (lower relative FOS) slip potential based on numerically predicted stress:

$$FOS = \frac{C + \sigma_n \cdot \tan\theta}{\tau} \quad (6)$$

where it is assumed for this formulation that C (cohesion) = 1 MPa and θ (friction angle) = 30˚.

A best-fit plane to the events following the shallow southeast trend along seismic source locations was evaluated (with a dip/dip direction of 25˚/139˚), and the FOS calculation was made for every zone in the FLAC3D numerical model for the March 2023 simulated extraction stage (corresponding to the month of the floorburst event). A horizontal section at 1,185 mbgs showing a contour of the calculated FOS, based on the resolved σ_n and τ along a 25˚/139˚ plane, is provided in Figure 16. Also plotted in this figure are two seismic event locations having occurred in March 2023 that had ML > –0.5. The contour illustrates that there was an elevated susceptibility to potential slip behaviour predicted in the numerical model along the presumed structural corridor within the vicinity of the 1,185 mbgs proximal to the location of the floorburst.

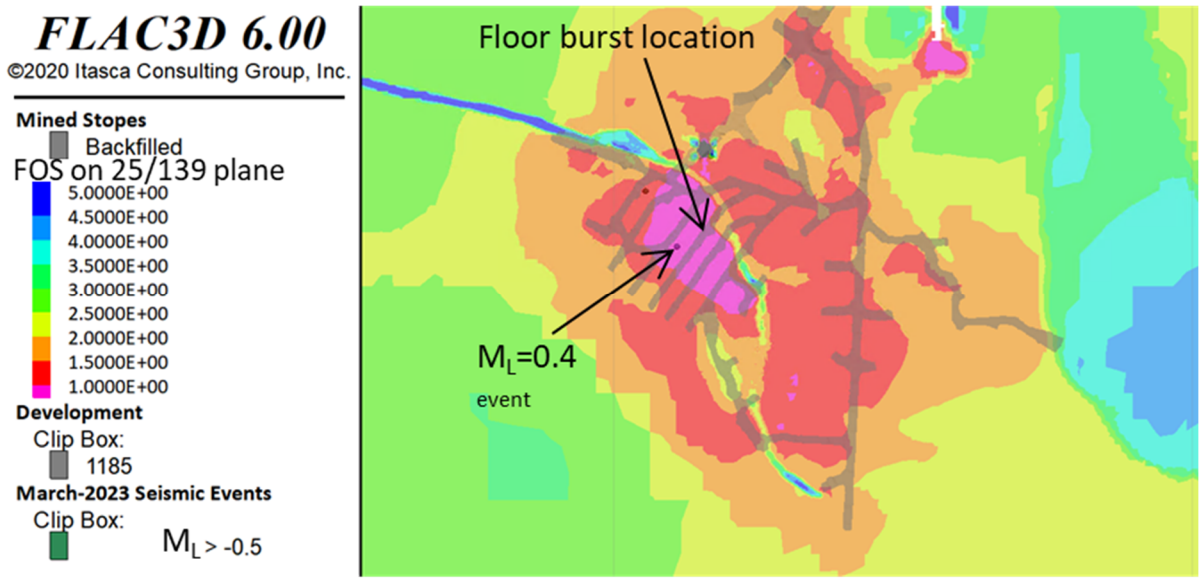

Figure 16 Horizontal section just below 1,185 mbgs showing a contoured FOS calculated from the resolved σ_n and τ along a 25˚/139˚ plane

4 Summary and discussion of next steps

Following the occurrence of a floorburst event, the case study mine halted production in the area until mechanistic analyses could resolve causal factors. Initial inspections and data review identified a conceptual model of slip on shallow dipping structures. A robust study involving seismic data analyses and numerical

stress modelling has verified the conceptual model. Seismic data analyses, including seismic moment tensor inversion, have resolved a slip mechanism with failure orientations aligned with the observed shallow dipping structures. The spatial distribution of events in the area also supports a planar trend evidencing a previously unidentified structural corridor. A global stress model has been developed and calibrated in order to assess stress loading conditions in the area of interest. Model results verify observational damage data and demonstrate elevated slip potential on the planar trend. The study concluded that an unidentified structural corridor was adversely exposed to mining-induced stress in a sill pillar, which drove slip failure.

The geological controls on this hazard domain were unknown at the time of the study and the following are hypothesised contributors:

- Locally the rock mass competency and/or intact material strength and stiffness may exceed more typical conditions observed throughout the mine. This allows for conditions with elevated stress accumulation prior to damage onset and contributes to the elevated intensity of seismic ground reaction (more brittle conditions). Exploring this hypothesis further will require additional site characterisation efforts to overcome uncertainties pertaining to intact material strengths.
- Locally elevated loading conditions may contribute to elevated seismic response. The area of interest is bound by weak ultramafics to the south and a graphite zone to the north, so the floorburst domain may act locally as a stress riser volume due to material strength and stiffness competencies. Exploring this hypothesis further will require further investigation of in situ stress conditions. This could be based on numerical model efforts with reliance on improved confidence in domain material properties (particularly intact material strengths), additional site characterisation efforts to overcome uncertainties pertaining to intact material strengths and/or in situ stress testing.

An additional causal factor not described in this paper but identified by broader seismic data analyses was that blasts exceeding 3,000 tonnes increase the potential for large events. This was implicitly evidenced in this paper from the two discrete events of increased seismic activity and large events following each of the two > 6,500 tonne stope blasts.

The study outcomes identified recommendations for actionable tasks including:

- targeted intact material testing and rock mass characterisation to further understand the local domain with apparent stress riser conditions
- updates to the geological model with a focus on structural conditions
- review of seismic system array design and expansion plans with the objective of increasing system sensitivity
- routine seismic data analyses and numerical stress model updates as new observational data continue to become available
- simulation of future mine plans to forward predict seismic hazards and provide geotechnical constraints for strategic sequencing and planning.

References

Hoek, E, Kaiser, P & Bawden, W 1995, *Support of Underground Excavations in Hard Rock*, A.A. Balkema, Rotterdam.

Itasca Consulting Group 2016, *FLAC3D Version 6.0 Reference Documentation*, Itasca Consulting Group.

Kalenchuk, K 2022, 'Predicting mine-wide seismogenic risk with confidence using calibrated numerical models', presentation at RaSiM 10: Rockbursts and Seismicity in Mines, Tucson, 26–28 April 2022.

Kalenchuk, K & Dadashzadeh, N 2022, 'The application of appropriately complex in situ stress for numerical modelling in geomechanics', presentation at the Sixth Peruvian Geoengineering Seminar, Lima.

Martin, D 1994, *The Strength of Massive Lac du Bonnet Branite Around Underground Openings*, PhD thesis, University of Manitoba, Winnipeg.